Effect of the individual layer thickness on the transformation of Cu/W nano-multilayers into nanocomposites

A.V. Druzhinin[a, b, c], D. Ariosa[d], S. Siol[a], N. Ott[a], B.B. Straumal[b, c, e], J. Janczak-Rusch[a], L.P.H. Jeurgens[a], C. Cancellieri[a, *]

[a] Empa, Swiss Federal Laboratories for Materials Science and Technology, Laboratory for Joining Technologies and Corrosion, Überlandstrasse 129, Dübendorf CH-8600, Switzerland

[b] National University of Science and Technology «MISIS», Leninsky prospect 4, Moscow 119049, Russian Federation

[c] Institute of Solid State Physics and Chernogolovka Scientific Center, Russian Academy of Sciences, Moscow district, Academician Ossipyan str., Chernogolovka 142432, Russian Federation

[d] Instituto de Física, Facultad de Ingeniería, Universidad de la República, Herrera y Reissig 565, C.C. 30, Montevideo 11000, Uruguay

[e] Karlsruhe Institute of Technology (KIT), Institute of Nanotechnology, Hermann-von-Helmholtz-Platz 1, Eggenstein-Leopoldshafen 76344, Germany

ARTICLE INFO

Keywords:
Cu/W nano-multilayers
Microstructure
Interface stress
Residual stress
Nanocomposite

ABSTRACT

Thermal treatment of nano-multilayers (NMLs) constituted of alternating immiscible metals, like W and Cu, can evolve in a nanocomposite (NC) with tailored mechanical, electrical and/or thermal properties. The NML-to-NC transformation can result in unique material properties of the resulting NC, which can hardly be achieved by conventional composite fabrication. In this paper, we systematically study the role of the individual Cu and W layer thicknesses in Cu/W NMLs on the diffusion, internal stress evolution and resulting NC microstructure upon heating by X-ray diffraction, high-resolution scanning electron microcopy and Auger electron spectroscopy. In the as-deposited state, a strong compressive stress state of Cu and W is observed, which is governed by a dominating interface stress contribution of the Cu{111}/W{110} interfaces of $11.25 \pm 0.56\,J/m^2$. Isothermal annealing of the as-deposited NMLs with different Cu and W layer thicknesses yields to the formation of nets of Cu protrusions on the NML surface, acting as a stress relaxation mechanism, which becomes thermally activated at 400 °C. The kinetics of Cu surface outflow are governed by the initial Cu/W stress state and the individual layer thickness ratio. During annealing at 700–800 °C, the Cu surface particles diffuse back into the volume of the near stress-free NML (dissolution), which defines the onset of accelerated degradation of the nanolaminated structure by thermal grooving, eventually forming a NC. The thickness ratio of Cu and W layers is shown to strongly affect the onset of the NML-to-NC transformation and the final NC microstructure.

1. Introduction

Nano-multilayers (NMLs) and nanocomposites (NCs) are functional nano-architectures, whose mechanical, chemical and/or physical properties can be tailored by smart microstructural and interfacial design [1]. According to definition, at least one of the phase constituents in a NML or NC should have a dimension in the nanometer range and, consequently, the resulting functional properties are governed by size-effects, as well as by the atomic and chemical structure of the internal phase boundaries [2]. Thermal, optical and/or mechanical properties of NMLs are typically tailored by controlled variation of the interface structure and individual layer thicknesses [3–5]. Analogously, the properties of NCs can be tuned by controlled variation of the relative volume fractions and sizes of the constituent phases to improve e.g. the mechanical strength while maintaining a good thermal conductivity [6,7].

Physical Vapour Deposition (PVD) is a common technique to fabricate NMLs, since it offers precise control of e.g. the chemical composition, individual layer thicknesses and modulation periodicity [8]. Nanocomposites of inorganic (e.g. metals, oxides, nitrides) and organic (e.g. polymers) phase constituents can be produced by various methods, such as cold spray, sol gel, spark plasma sintering or CVD [9]. NCs constituted of two immiscible metals by PVD deposition techniques are also reported, either directly by co-sputtering or by alternating layer deposition steps with subsequent high-temperature annealing [6,10,11]. Interestingly, sputter-deposited NMLs of alternating nano-layers of two immiscible metals can be transformed into a NCs by thermal annealing [11–14]. The microstructural design of the building blocks of the NML provides a defined route for tailoring mechanical properties [10,15,16], electrical [17] and thermal [18] conductivities, as well as the coefficient of thermal expansion [19] of the transformed NC. However, NMLs and NCs produced by PVD deposition techniques generally exhibit large internal residual stresses, which can compromise their thermal stability and ultimate performance [20]. As demonstrated in Ref. [21], the NML-to-NC transformation in Cu/W NMLs upon annealing is preceded

* Corresponding author.
E-mail address: claudia.cancellieri@empa.ch (C. Cancellieri).

by outflow of the confined Cu metals to the NML surface, which can be exploited to achieve a functional bond between two base materials. To this end, the base substrates (Mo) were pre-coated with the Cu/W NML; subsequent joining at 750 °C resulted in a solid joint between the base materials with the joint zone being composed of a spheroidized Cu/W nanocomposite with an accumulation of Cu at the contact interface [21].

Tungsten-based NMLs are also relevant for many microelectronic applications as W often acts as a chemically-inert diffusion barrier between Si-based devices and Cu interconnects [22–24].

Cu/W NMLs have been extensively investigated in their structure and internal stress [25–27]. For example, Refs. [11,14] investigated the thermal stability of Cu/W NMLs with 100 repetitions of a bilayer unit, constituted of one Cu and one W nano-layer with an individual thicknesses of 5 nm. The onset temperature for the degradation of the NML into a NC was found to be governed by a stress-relaxation-driven diffusion processes, which were independent of the parent substrate. The Cu/W NML-to-NC transformation at high temperatures (~800 °C) can be accompanied with Cu surface outflow at lower temperatures (~500 °C) through a stress relaxation process. Previous investigations of the NML-to-NC transformation were only performed for fixed W and Cu layer thicknesses of 5 nm each [11,14]. The individual layer thickness directly scales with the average grain size [14] so by changing the Cu and W thickness is like changing the grain size of the NML constituents. In the current study, the W and Cu layer thicknesses were varied between 3–10 nm (for a fixed number of 20 repetitions) to reveal the effect of the NML design and intrinsic stress state on the NML-to-NC transformation kinetics and the resulting NC microstructure. To this end, the microstructure and internal stress states of Cu and W in the annealed Cu/W NMLs were investigated after successive stages of the NML-to-NC transformation by a combined experimental approach using X-ray diffraction, high-resolution scanning electron microcopy and Auger electron spectroscopy. As such, the different stages of NML-to-NC process were revealed, also disclosing the crucial role of the individual Cu and W nano-layers thicknesses on the transformation behavior.

2. Experimental methods

Cu/W nano-multilayers were deposited at room temperature on 10×10 mm^2 polished α-Al_2O_3 (0001) single-crystalline wafer substrates (i.e. sapphire-C wafers) by magnetron sputtering in an ultrahigh vacuum chamber (base pressure $< 10^{-8}$ mbar) from two confocally arranged, unbalanced magnetrons equipped with targets of pure W (99.95%) and pure Cu (99.99%). Before insertion in the sputter chamber, the sapphire substrates were ultrasonically cleaned using acetone and ethanol. Prior to deposition, possible surface contamination on the α-Al_2O_3 (0001) substrate was removed by Ar+ sputter cleaning for 5 min applying an RF Bias of 100 V at a working pressure of 1.6×10^{-2} mbar. The RF Bias was maintained during the NML deposition at a working pressure of approximately 5×10^{-3} mbar. First, a 25 nm thick W buffer layer was deposited on the sputter-cleaned substrate. Next, NMLs consisting of 20 repetitions of a Cu/W building block were deposited on top. Different NML configurations were prepared by controlled variation of the Cu and W nano-layer thicknesses in the Cu/W building block: i.e. 3 nm Cu/3 nm W (3Cu/3W), 10 nm Cu/3 nm W (10Cu/3W), 3 nm Cu/10 nm W (3Cu/10W), 5 nm Cu/5 nm W (5Cu/5W), 10 nm Cu/10 nm W (10Cu/10 W). To study the successive stage of the NML-to-NC transition, the samples were isothermally annealed for 100 min at various temperatures in the range of 400–800 °C under high vacuum conditions ($< 10^{-5}$ mbar), while applying a heating rate of 20 K/min.

Cross-sectional cuts of the as-deposited and annealed NMLs were prepared by a Hitachi IM4000Ar ion milling system (acceleration voltage of 6 kV, discharge voltage of 1.5 kV, a swing angle of ±30°) and by a FEI Helios NanoLab 660 SEM/FIB. Planar and cross-sectional imaging was performed by high-resolution SEM (HR-SEM) analysis using a Hitachi S-4800 instrument. Chemical analysis of the annealed NML surfaces was performed by Auger electron spectroscopy (AES) using a Physical Electronics PHI-4300 SAM system equipped with a cylindrical mirror analyzer (CMA; constant relative energy resolution $\Delta E/E$ of 0.3%) and a coaxial electron gun operating at 5 keV with an emission current of 50 μA. AES analysis of surface particles on the annealed NML surfaces was conducted with a lower beam current of 2.2 nA, resulting in an analysis spot of about 300 nm. Each Auger spectra was recorded for 60 min with a kinetic energy step of 1 eV and an accumulation time of 40 ms/eV (50 iterations). All spectra were processed with the use of the MultiPak V6.1A program package (differentiation with 9 points, Savitzky–Golay smoothing with 5 points).

A Bruker D8 Discover X-ray diffractometer operating in Bragg-Brentano geometry was used to measure 2θ scans for the as-deposited and annealed NMLs. All annealed NMLs were measured *ex-situ* after cooling down to room temperature (RT). Diffraction patterns were recorded in a 2θ range from 10° to 90° using Cu K $\alpha_{1,2}$ radiation at 40 kV/40 mA. Texture analysis was performed by acquiring pole figures for the Cu{111} and W{110} families of planes. Stress analysis was carried out using the Crystallite Group Method (CGM) [28], suitable for highly textured systems, like in the present case (see Part II in Supplementary materials).

3. Results

3.1. Microstructure of as-deposited Cu/W NMLs

In Fig. 1, SEM images of a typical surface morphology and cross-sectional view of an as-deposited Cu/W NML are presented (as an example the 10Cu/10W NML is chosen). The as-deposited NML surfaces

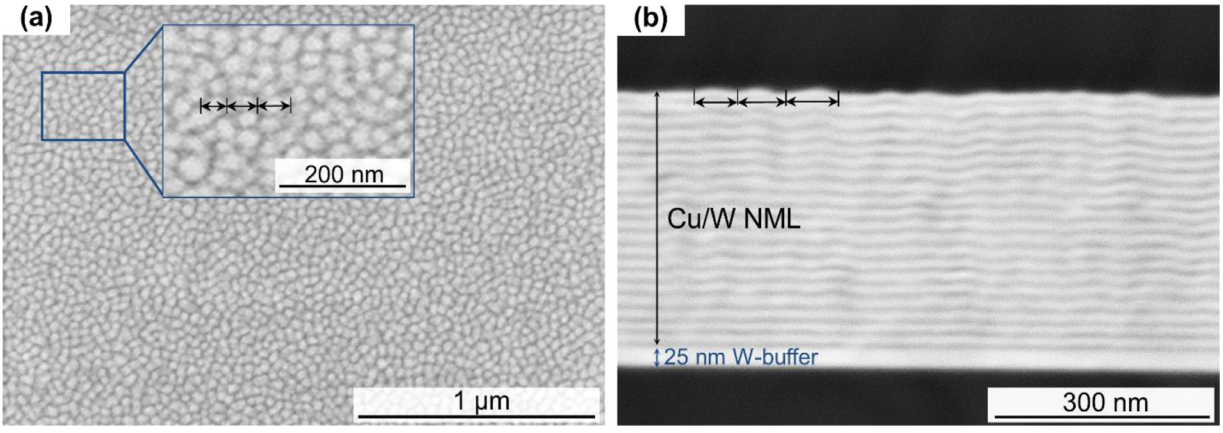

Fig. 1. SEM images of the 10Cu/10W NML in the as-deposited state: (a) planar view and (b) cross-sectional view. Insert in (a) shows magnified wave-like structure of deposited layers (typical length indicated by arrows).

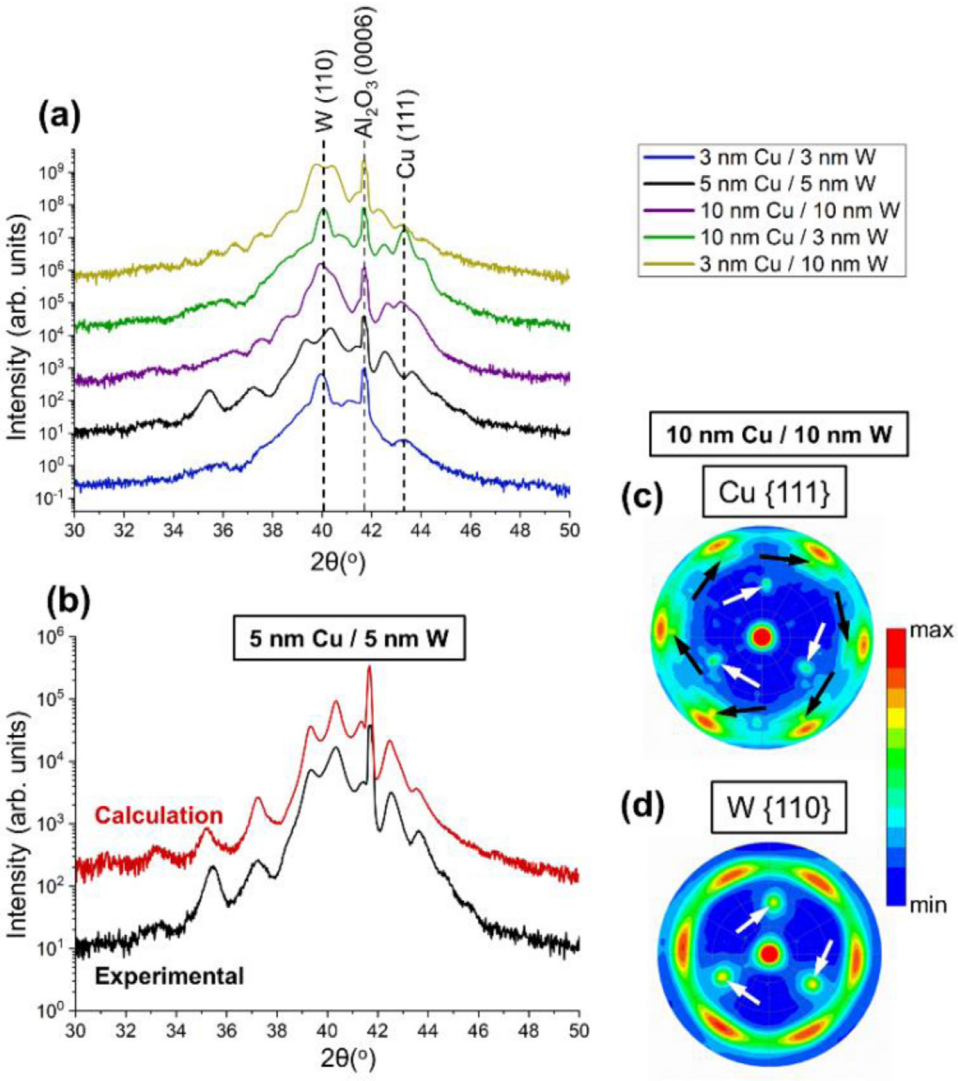

Fig. 2. XRD analysis of as-deposited NMLs with different Cu and W layer thicknesses (intensity plotted in a logarithmic scale): (a) Overview of the region indicating the presence of satellite peaks imposed by the NML structure (θ–2θ scans). The position of the bulk W(110) and Cu(111) reflections are indicated with dashed lines. (b) Comparison of a calculated and measured satellite peak structure for the as-deposited 5Cu/5W NML. (c,d) Pole figures of the Cu{111} and W{110} families of planes for the as-deposited 10Cu/10W NML, revealing an in-plane and out-of-plane texture with a crystallographic orientation relationship Cu{111}<–101>||W{110}<–111>.

show a uniform surface morphology without any distinct artifacts, such as cracks or voids [27]. The cross-sectional analysis reveals that the bottom nano-layers deposited during first cycles of deposition are relatively flat and well-aligned with the W buffer layer. However, successively deposited nano-layers exhibit an increased waviness and have less lateral thickness uniformity. A decrease of layer thickness uniformity for successive nano-layer deposition steps was also observed for other NML systems, such as Zr/Nb [3], Cu/V [29], NbN/MoN [30], WS_2/MoS_2 [31] and Cu/W [11,27].

The crystalline structure of as-deposited NMLs was investigated by X-ray diffraction as illustrated in Fig. 2a. A set of satellite peaks around the bulk (characteristic for bulk Cu and W crystals) (110)W and (111)Cu reflections in the 2θ range between 30° and 50°, which originate from the periodic layer structure (artificial superlattice) [11], is visible in Fig. 2a. Similar superlattice modulations were observed for NMLs of other systems (Zr/Nb [3], TiAl/TiAlN [32], Au/Ni [33]). An approach for the model calculation of artificial superlattices in Cu/W NMLs was previously introduced in Ref. [11]. In the present study the model in [11] was improved in order to include moderate interface roughness: the total multilayer diffraction intensity expression is calculated and then averaged over both, Gaussian subatomic internal displacements and Poisson distributed layer thicknesses. From the adjustment with experimental data, internal disorder and lattice parameters of 0° tilt angle for Cu(111) and W(110) reflections (used for the Cu/W stress calculation) were derived. The intra-layer displacement disorders in Cu and W layers are presented in Section 3.3, together with stress values in the respective layers. Detailed description of the model is in the Supplementary material, Part I.

In Fig. 2c and d, pole figures of the Cu{111} and W{110} family of planes for 10Cu/10W as-deposited NML are presented. Both the Cu and W pole figures display six-fold symmetrical high-intensity poles which indicates a pronounced in-plane texture of the grown NMLs: Cu poles are positioned closely to $\psi = 70.53°$ which is the angle for the {111}Cu family of planes, while W poles belong to the {110} family with $\psi = 60°$. While, for cubic crystals, <111> directions are 3-fold and <110> ones are 2-fold symmetric, the twinning due to the mutual adaptation of the fcc Cu(111) planes with the bcc W(110) ones produces an effective 6-fold symmetric pattern in the pole figures. In addition, for the W(110) this mutual adaptation produces 12 spots distributed in 6 close doublets that are, each of them, 10.52° apart. Each double spot will be centered around an in-plane Cu[2–21] direction among the 6 possible directions. The observed unusual azimuthal extension of W(110) poles is related to these adjacent double spots (not resolved in the pole figure), which appear as single broad spots in the circle at the polar angle 60° (see details in the Supplementary material, Part III). The central poles at $\psi = 0°$ correspond to the W(110) and Cu(111) preferential growth planes. In addition, the W pole figure displays three less intense poles around $\psi = 36°$ (highlighted by white arrows in Fig. 2d). These reflections originate from the W buffer layer, which possesses a preferred [111] growth direction. Additional poles of low intensity in the Cu pole figure, around

$\psi = 37^\circ$ and $\psi = 63^\circ$ are the traces of W (110) vs (111) (highlighted by white arrows in Fig. 2c) and (2–13)Al_2O_3 planes (highlighted by black arrows in Fig. 2c). In conclusion, the as-deposited NMLs display both in-plane and out-of-plane texture with the crystallographic orientation relationship Cu{111}<–101>||W{110}<–111>.

3.2. Microstructure of annealed Cu/W NMLs

As demonstrated in our previous studies on the thermal stability of Cu/W NMLs with fixed layer thicknesses of 5 nm Cu and 5 nm W (100 bilayer repetitions) [11,14], the NML is completely transformed into a nanocomposite structure after 100 min of isothermal annealing at 800 °C. An Arrhenius analysis of the transformation kinetics by *in-situ* high-temperature XRD indicated that the NML-to-NC transition is governed by the mass transport of W atoms along internal interfaces (e.g. phase and grain boundaries) in the annealed Cu/W NMLs [11,14]. The microstructures of investigated NMLs with different Cu/W thicknesses, after isothermal annealing at 800 °C, are shown in Fig. 3, where a comparison of surface and cross section morphologies is presented. The 10Cu/10W NML is the only NML that still shows some remnants of a NML structure, although with evident signs of a partial transformation into a NC (Fig. 3e). As it is evidenced from Fig. 3, the NC microstructure depends on the initial design of the Cu/W NML: the W grains have recrystallized into a more spherical shape for NMLs with the combination of thick Cu and thin W layers (e.g. 10Cu/3W NML in Fig. 3c). Surprisingly, the Cu{111}<–101>||W{110}<–111> orientation relationship is conserved in all NCs, although with a less intense signal compared to the as-deposited state (Fig. 3f).

XRD analysis of annealed NMLs in the present study (20 bilayer repetitions with different individual Cu and W layer thickness) also shows a gradual transformation of the studied Cu/W NMLs into a NC structure at $T \geq 700$ °C, as evidenced by the gradual disappearance of the satellite peaks (Fig. 4) and the presence of two distinct bulk W(110) and Cu(111) reflections (in accordance with Ref. [11]). In Fig. 4, a comparison of the satellite peak structure evolution with annealing temperature in two different NMLs (10Cu/3W and 10Cu/10W) is shown. In the 10Cu/10W NML annealed at 800 °C the θ–2θ scan still shows minor traces of satellite peaks (highlighted by arrows in Fig. 4b), while for the annealed 10Cu/3 W NML only bulk (110)W and (111)Cu reflections are present (Fig. 4a). This is in accordance with a partially destroyed layer structure in the 10Cu/10W NML (Fig. 3e).

SEM analysis of the NML surfaces after annealing at different temperatures in the range of 400–700 °C, indicates that the onset of the NML-to-NC transformation is preceded by the formation of randomly distributed protrusions on the outer NML surface (Fig. 5a). Local chemical analysis by AES confirms that these protrusions are pure Cu crystals (see Part VI of the Supplementary material). The majority of the particles, after annealing at 400 °C, has a rod or whisker shape (Fig. 5b,c), while at 600 °C they transform into equiaxed bulk crystals (hillocks) (Fig. 5d and e). As reflected in Fig 5b, nuclei of Cu protrusions initially originate in the volume of the NML structure and subsequently grow by fast supply of Cu atoms along the pathways formed by localized ruptures in the NML film (cross sectional view will be presented in Fig. 6c). However, such ruptures of the NML structure without Cu outflow (Fig. 5g) are also found in thermally treated NMLs (mainly in 3Cu/10W and 10Cu/10W NMLs).

In Fig. 6, STEM dark field images with EDX line-scan analysis of a region underneath a Cu whisker root (5Cu/5W NML annealed at 500 °C) are presented. It follows that not all the NML volume is involved in the rupture formation and almost a half of the NML structure is preserved and intact (Fig. 6b and c). The ratio of the Cu whisker volume to the total volume of the NML (Fig. 6b) is quite large denoting extensive in-plane Cu mass transport from the NML exterior to the whisker root. STEM EDX line scans (Fig. 6d) display the change in the structure of the alternating Cu/W layers: for the L1 line, the initially periodic layer structure compared to the one shown on the L2 line is lost moving towards the whisker root.

A variation in the quantity of Cu protrusions on the NML surface is observed among NMLs with different individual layer thicknesses. In Fig. 7, low magnification SEM images of several annealed NML surfaces

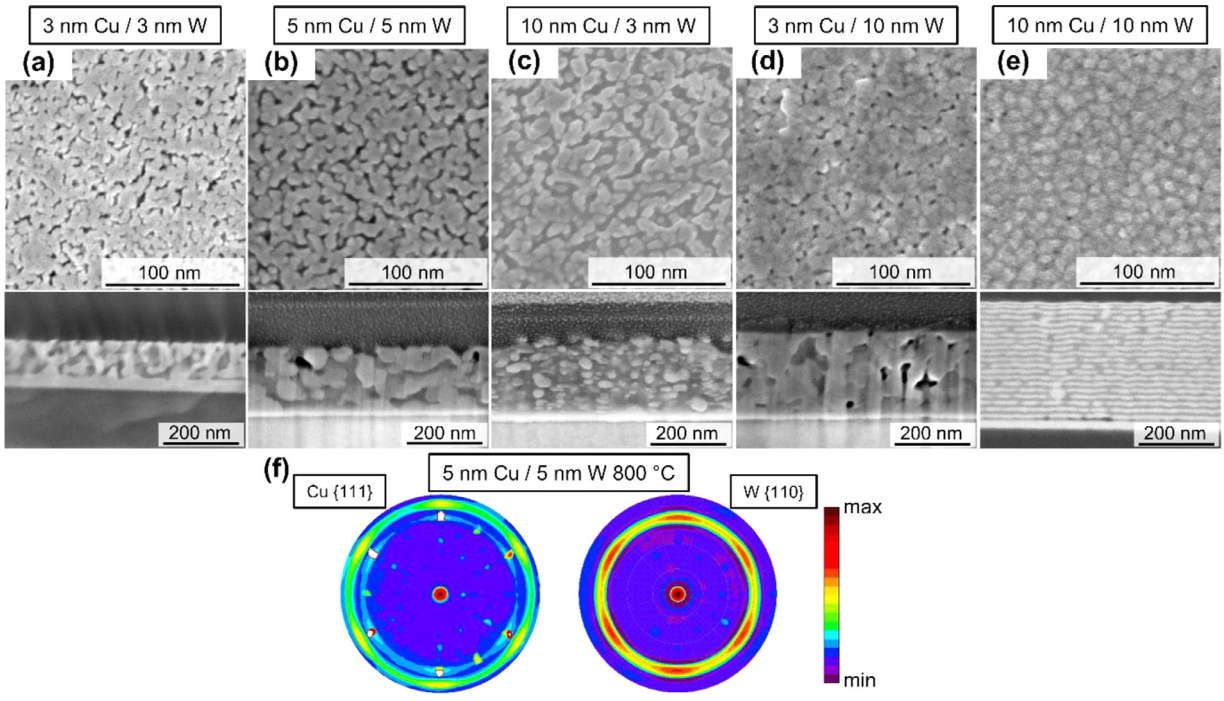

Fig. 3. SEM micrographs (both in planar and cross-sectional view) of the Cu/W NMLs after annealing at 800 °C, evidencing a transformation of nano-multilayer (NML) into a nanocomposite (NC) structure. The NMLs in (a–d) are completely transformed into a nanocomposite structure. The cross sectional view of the annealed 10Cu/10W NML in (e) still shows the remnants of a NML structure (image made in BSE signal). (f) Pole figures of the Cu{111} and W{110} families of planes, indicating the conservation of a Cu{111}/W{110} texture after nanocomposite formation (by the example of 5Cu/5W NML).

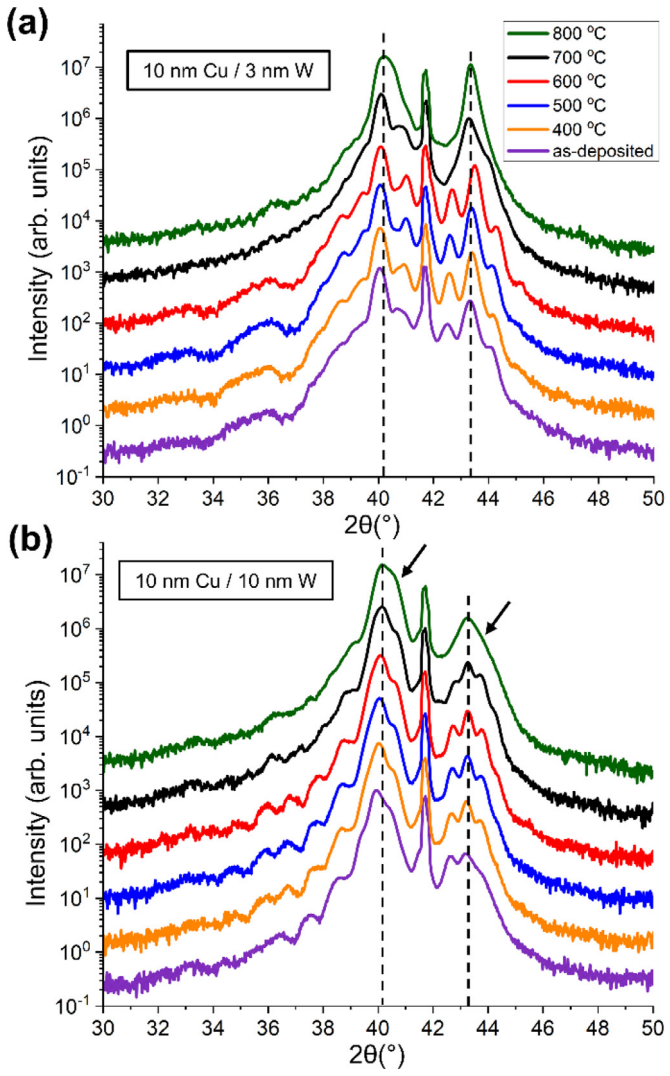

Fig. 4. Evolution of satellite peak structure as a function of annealing temperature in (a) 10Cu/3W and (b) 10Cu/10W NMLs. Positions of distinct bulk W(110) and Cu(111) reflections are indicated by dashed lines.

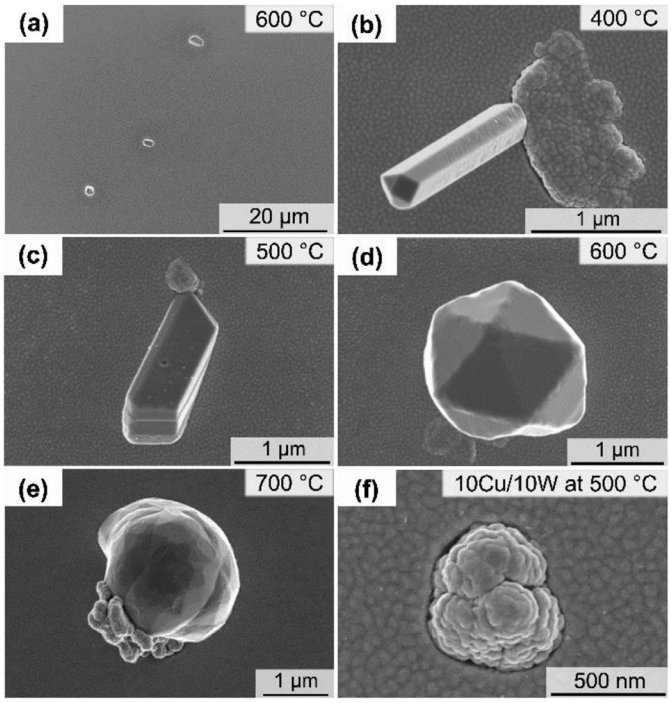

Fig. 5. Microstructural evolution of the Cu/W NML surface upon annealing for the (a–e) 5Cu/5W and (f) 10Cu/10W NMLs. (a) Low-magnification SEM image of the NML surface after annealing at 600 °C, indicating the presence of Cu protrusions on the surface. (b–e) High-magnification images of Cu protrusions on the annealed 5Cu/5W NML surfaces. (g) Rupture of the NML structure without Cu outflow for the 10Cu/10W NML annealed at 500 °C.

(3Cu/3W, 5Cu/5W, 10Cu/10W) are presented. No traces of microstructure modifications (ruptures of the NML structure with or without Cu outflow) are found in the 3Cu/3W NML after annealing at 400 °C. On the contrary, the annealed 10Cu/10W (and in 3Cu/10W as well) NML surfaces already show several ruptures without Cu outflow at 400 °C (visible Cu outflow at 500 °C) (Fig. 7). For the annealed 5Cu/5W and 10Cu/3W NMLs, a gradual increase of both the density and size of Cu protrusions are observed with increasing annealing temperature, attaining an average particle size of 2–2.5 μm at 700 °C.

For 10Cu/10W NMLs, the Cu surface particles grow prevalently in size, but not in quantity, with increasing annealing temperature: at 700 °C, the largest Cu particles with an average size of roughly 4–5 μm are found, although their density is the lowest among all investigated NMLs. For 10Cu/10W NMLs, with the increase of annealing temperature, Cu particles grow prevalently in size, but not in quantity: at 700 °C, Cu particles in 10Cu/10W NML are the largest in size (~4–5 μm), but the lowest in amount among all investigated NMLs. Finally, the 3Cu/3W NMLs display a relatively weak outflow in the range of 400–600 °C, but develop a relatively large density of surface particles (with a mean size of about 1 μm) after the annealing at 700 °C. These observations show that the kinetics of Cu surface mass migration upon thermal treatment (onset of outflow, change in size and amount of particles) not only depends on the internal stresses in the layers, but also on the individual Cu and W layer thicknesses (see Section 4.2 for more details).

Strikingly, it was observed that for annealing temperatures $T >$ 700 °C, previously formed Cu surface protrusions, start to dissolve back into the NML. This phenomenon is already observed at an annealing temperature of 700 °C for the 10Cu/3W NML. All other NMLs required a somewhat higher annealing temperature in the range of 700–800 °C to activate the dissolution of Cu surface protrusions. A combined SEM-AES analysis of the 10Cu/3W NML surface in the vicinity of a Cu surface protrusion for two different stages of annealing at 700 °C is shown in Fig. 8. In Fig. 8a an intermediate process of the Cu dissolution process is shown. After complete dissolution of the Cu surface protrusion, a contrast difference in the SEM image between the originally area covered with the Cu protrusion area (brighter area in Fig. 8c), and its surrounding area (darker area in Fig. 8c) remains. However, quantitative AES analysis shows no apparent differences in surface composition between the bright and dark areas, which suggests that the contrast in the SEM images originates from slight differences in surface topography. Importantly, local AES analysis in region 2 in Fig. 8c reveals small black spots concentrated at W grain boundaries (Fig. 8d), which correspond to Cu enrichments. Similar black spots are found in the annealed 3Cu/3W (at 700 °C) and 10Cu/10W (at 800 °C) NMLs. A cross sectional view of the annealed 10Cu/3W NML at some distance from the dissolved Cu region (as indicated in Fig. 8a), reveals an intermediate stage of the NML-to-NC transformation (Fig. 8b).

3.3. *Evolution of Cu and W stress upon thermal treatment*

The residual stress of the Cu and W layers is derived by room temperature *ex-situ* XRD analysis. Since all NMLs are highly textured, the Crystallite-Group Method (CGM) was used for the stress calculations [28,34]. The CGM is a variant of the commonly applied "$\sin^2\psi$" method that accounts for the presence of a strong texture. A particular group of

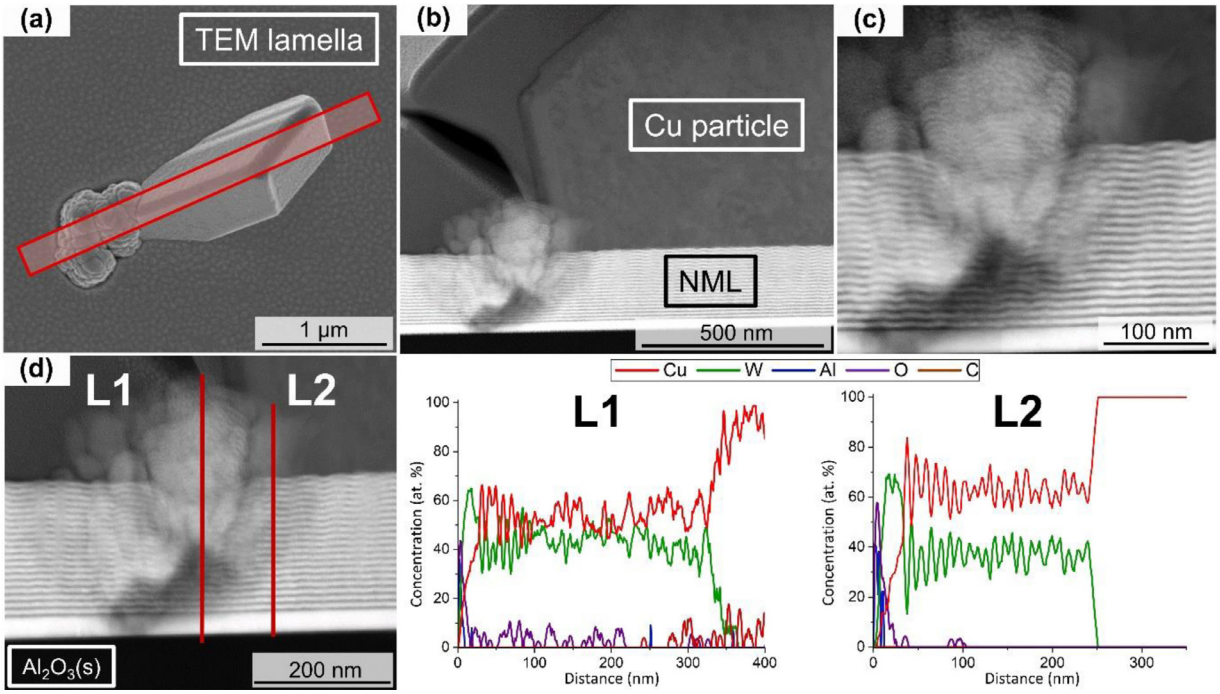

Fig. 6. STEM investigation of a Cu whisker area (5Cu/5W after 500 °C). (a) SEM image of the selected Cu whisker for STEM lamella preparation. (b) Low-magnification dark field image of the contact area between the Cu whisker and the NML structure. (c) High-magnification dark field image of a rupture of the NML structure at the whisker root. (d) Comparison of EDX line scans of the NML volume along two scanning directions in the region of the Cu whisker root.

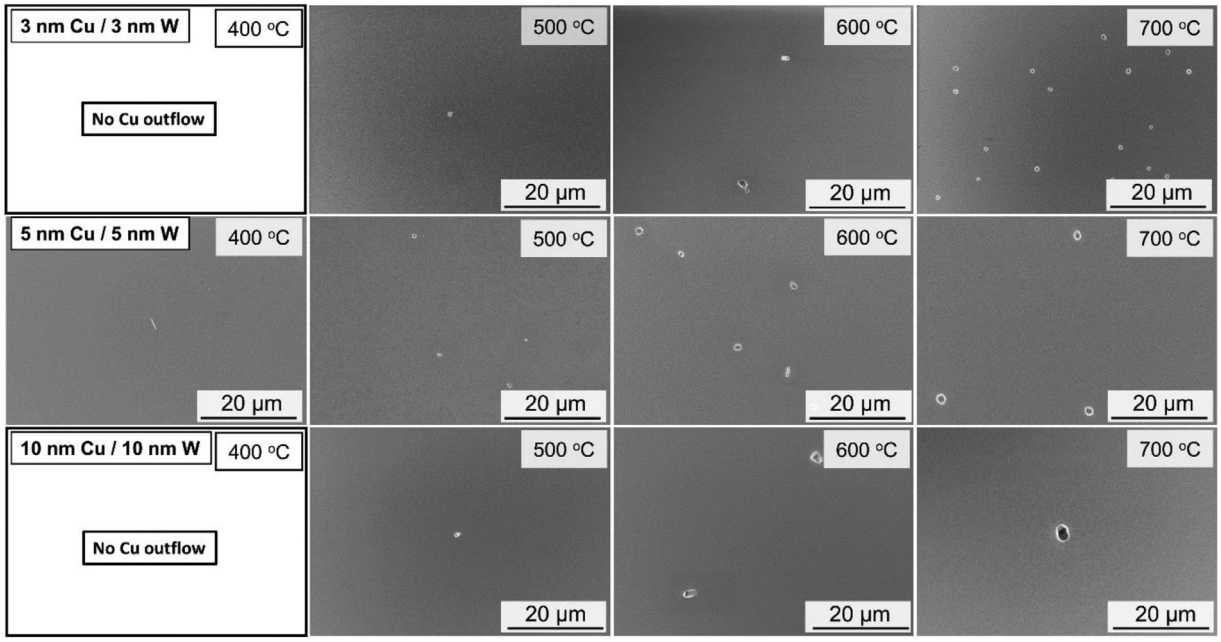

Fig. 7. Low magnification surface SEM images of 3Cu/3W, 5Cu/5W, 10Cu/10W NMLs after isothermal annealing in the range of 400–700 °C. No Cu particles were observed on the 3Cu/3W and 10Cu/10W NML surfaces after annealing at 400 °C.

crystallites with the same crystallographic orientation (crystallite group) is chosen, for which the measured lattice strain is averaged over all crystallites. When applying Hook's law to the case of thin films, the stress components (principal and shear) normal to the film surface can be taken zero: i.e. $\sigma_{33} = \sigma_{13} = \sigma_{23} = 0$. Moreover, for the case of an isotropic cubic film with an equal-biaxial stress state it holds that: $\sigma = \sigma_{11} = \sigma_{22}$. In the present study, the Cu<11−2> and W<1−21> group crystallites were selected for the CGM residual stress analysis [14]. Details about the stress analysis conducted on multiple reflections using CGM can be found in the supplementary materials (Figs. S3 and S4).

Fig. 9a shows the evolutions of the residual stresses in Cu and W for various individual Cu and W layer thicknesses after annealing at different temperatures. In the as-deposited state, the Cu and W layers all exhibit a compressive stress, which magnitude depends on the individual Cu and W layer thicknesses. Noteworthy, W layers in the as-deposited state exhibit a similar stress level (~−3.5 GPa) for all investigated NMLs, except for the NMLs with the thinnest Cu layers (3Cu/3W and 3Cu/10W NMLs) (see Fig. 9a lower panel). The highest compressive stress in W is found in the as-deposited 3Cu/3W NML (~−6.75 GPa). For the as-deposited 3Cu/10W NML, W possesses an intermediate stress state

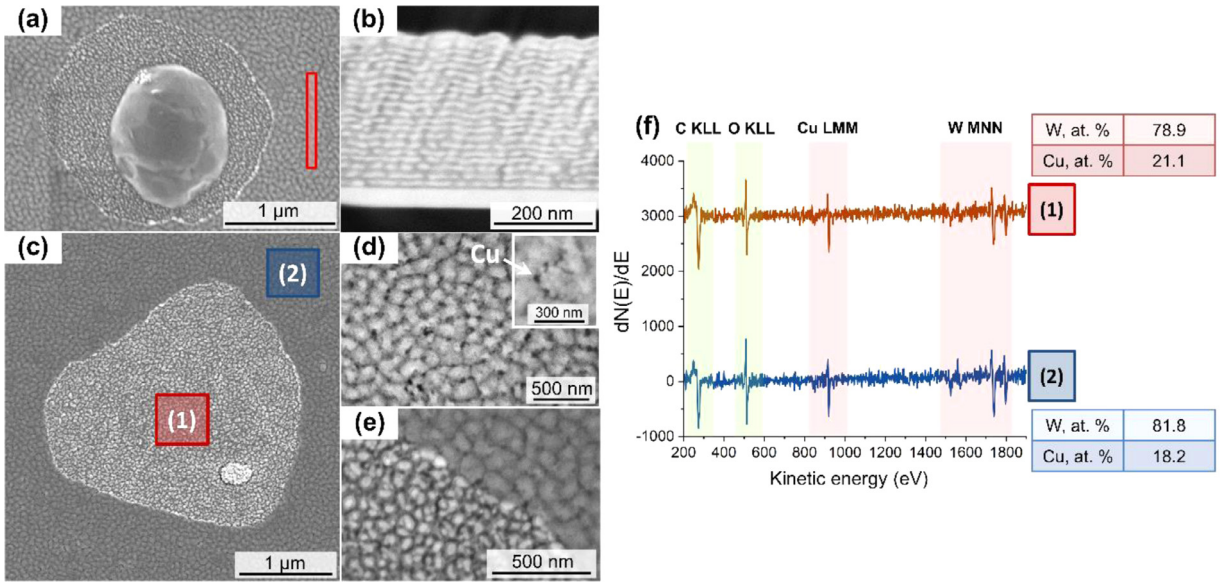

Fig. 8. Combined SEM-AES analysis of the NML surface of the 10Cu/3W NML in the vicinity of a Cu surface protrusion for different stages of annealing at 700 °C. (a) Intermediate stage of the Cu particle dissolution process, showing a shrinked Cu protrusion on the annealed NML surface. (b) Cross sectional SEM image of the annealed NML at some distance from the dissolved Cu region as indicated in (a), revealing an intermediate stage of the NML-to-NC transformation. (c) the identical area of (a) after complete dissolution of the Cu surface protrusion. (d,e) Magnified SEM images of the annealed NML surface at selected locations outside and inside the dissolved Cu protrusion region, respectively. The insert in (d) highlights tiny Cu enrichments (black spots). (f) AES spectra of regions 1 and 2, as indicated in (c), with the corresponding relative atomic concentrations of Cu and W.

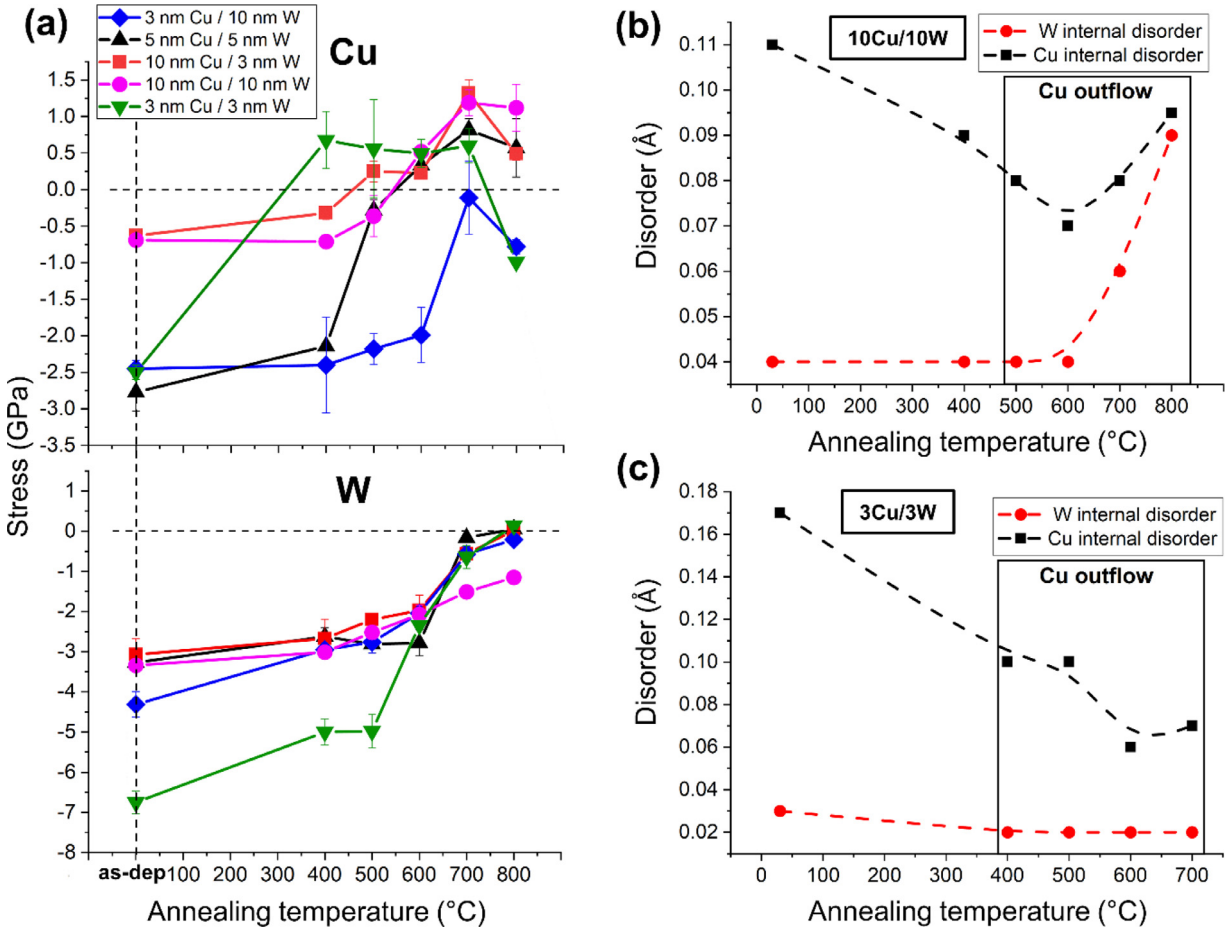

Fig. 9. Average residual stresses and internal displacement disorders in the Cu and W layers, as derived by XRD. (a) Residual stresses of Cu and W in the NMLs with various individual layers thicknesses after annealing at different temperatures, as measured after cooling down to room temperature. Error bars are derived from the linear fit of the lattice parameter as a function of $\sin^2\psi$. (b,c) Estimated internal displacement disorder within the Cu and W layers as function of annealing temperature for (b) the 10Cu/10W and (c) the 3Cu/3W NMLs, as derived from the XRD superlattice model calculation (see Supplementary material, Part I).

between 3Cu/3W and the other NMLs (lower panel of Fig. 9a). The stress evolution in W layers after thermal treatment shows a similar trend for all investigated NMLs, i.e. the residual stress gradually relaxes with increasing annealing temperature, resulting in a nearly unstrained state after annealing at 800 °C. Only the 10Cu/10W NML maintains a non-zero residual compressive stress after annealing at 800 °C. The temperature-stress evolution of W in the 10Cu/10W NML was found to be almost linear and predominantly governed by thermal expansion forces, as shown in Supplementary material, Part V. Remarkably, the 10Cu/10W NML preserves a high compressive W stress after 800 °C (NML-to-NC transformation is not completed; Fig 3e).

Cu layers exhibit a considerable spread in their stress values in the as-deposited state (upper panel of Fig. 9a). The Cu layers in the as-deposited 3Cu/3W, 3Cu/10W, 5Cu/5W NMLs possess a compressive stress of about −2.5 GPa, whereas the stress level for 10Cu/3W and 10Cu/10W NMLs, with the thickest Cu layers (10 nm), is much smaller (−0.75 GPa). As for W layers, the compressive stresses in the as-deposited Cu layers are relaxed upon high-temperature annealing. Cooling down after annealing at 700 °C results in a tensile stress in Cu. The residual stress in Cu (as measured at room temperature) after annealing at 800 °C is either compressive or tensile depending on the individual Cu and W thicknesses.

Fig. 9b,c shows the estimated internal displacement disorder within the Cu and W layers as function of the annealing temperature for the 10Cu/10W and 3Cu/3W NMLs (as derived from the XRD model calculations; the estimated internal disorder in the 5Cu/5W NML is provided in the Part IV of Supplementary material). The internal displacement disorder corresponds to the standard deviation of the random variation of interplanar spacings inside of each Cu and W layer along the normal to the NML surface (see Supplementary material, Part I). As follows, the internal disorder in Cu and W initially decreases with increasing annealing temperature in the range of 400–600 °C, and it is subsequently followed by a gradual increase in the range of 700–800 °C. Generally, the variation of internal disorder is less pronounced in the W layers (as compared to the Cu layers). As discussed in Section 4.2, the evolution of the internal disorders in Cu and W relates to the concurrent surface outflow of Cu

3.4. Determination of (111)Cu/(110)W interface stress

The total residual stress in PVD thin films deposited at room temperature generally arises from a superposition of coherency and deposition (growth) stresses [35]. Deposition stress originates from atom rearrangements and grain nucleation in the developing film during the deposition process (e.g. island nucleation, growth and coalescence; grain growth; diffusion of surface adatoms into grain boundaries). Coherency stress arises from the lattice mismatch between the substrate and the developing film at the substrate-film interface. A decrease of coherency stress with increasing film thickness is generally realized by the introduction of misfit dislocations at the interface beyond a certain critical film thickness [36]. Connected to the coherency stress, there is the stress generated by the interface between adjacent layers – interface stress, which is defined as the reversible work required to introduce elastically a unit strain at the interface between two phases [37]. The magnitude of interface stress has an important impact on the critical film thickness for misfit dislocations formation and consequently on the onset of intense coherency stress relaxation during film growth [37]. Interface stress generally induces an additional in-plane elastic strain in the volume of the thin film (on top of coherency and deposition strain), which becomes increasingly dominant with the decrease of the film thickness. Thus, for nanometer thick films, interfaces start to play a dominant role in the definition of the final stress state. The methodology developed by Ruud et al. [38] was applied to extract the Cu/W interface stress contribution in the investigated Cu/W NMLs, i.e.

$$\sigma_{SC} - \langle\sigma\rangle = 2f/\lambda, \quad (1)$$

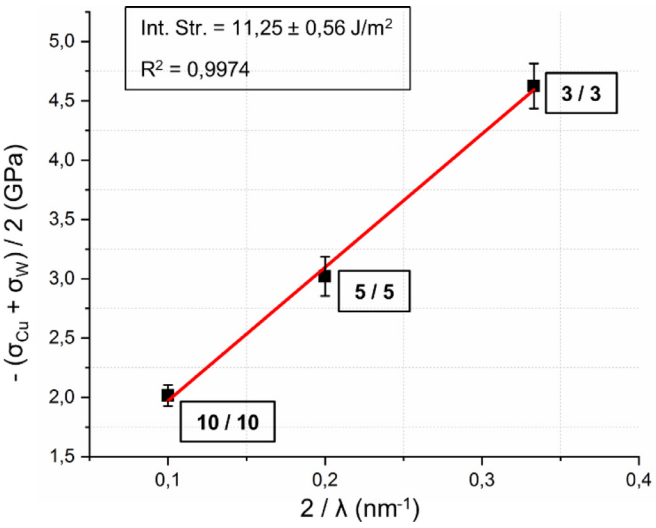

Fig. 10. The sum of determined Cu and W stresses plotted as a function of the inverse bilayer thickness for 3Cu/3W, 5Cu/5W and 10Cu/10W as-deposited NMLs. Value of interface stress (presented in the text box) is derived from the slope of the line fitted to the data points. Error bars are estimated on the basis of values derived from the *ex-situ* stress measurements.

where σ_{SC} is the average stress measured by substrate curvature, $\langle\sigma\rangle = \frac{(\sigma^{Cu}_{x-ray}+\sigma^{W}_{x-ray})}{2}$ is an average deposition stress (assuming that coherency stresses in bilayers with equal thick layers cancel out), λ^{-1} is the inverse bilayer repetition length and f is the interface stress.

As follows from Eq. (1), the interfacial stress contribution from all interfaces in a given NML system equals the difference between the average stress of the NML ensemble, as measured by substrate curvature, and the total NML deposition stress, as measured by XRD. In our case, the number of interfaces in the studied NMLs was kept constant (number of bilayer repetition was fixed at 20). Moreover, the maximum NML thickness does not exceed 400 nm (pertaining to the 10Cu/10W NML), while the sapphire substrate thickness is around 500 μm. It is thus assumed that the forces exerted by a NML film are negligible to produce an appreciable curvature of the substrate. A similar case was reported for the calculation of interface stress by the above mentioned model for the Ag/Ni NMLs (500 nm thick multilayers on a 360 μm Si substrate) [39], where stress values determined from the substrate curvature were considerably smaller than stresses measured by x-ray diffraction and thus did not significantly affect the interface stress determination.

Fig. 10 shows the total average deposition stress $\langle\sigma\rangle$, as calculated using the stress values in the as-deposited NMLs with equivalent Cu and W layer thicknesses (Fig. 9a), plotted as a function of $2/\lambda$. The slope of the line fitted to the data points in Fig. 10 gives a mean interface stress value of 11.25 ± 0.56 J/m^2 for Cu(111)/(110) W interfaces. The absolute value of the interface stress in the studied Cu/W NMLs is of opposite sign and significantly larger than the interfacial stress in other systems: −2.27 ± 0.67 J/m^2 for (111) Ag/Ni [38], −3.19 ± 0.43 J/m^2 for (111) Ag/Cu [40] and −1.80 J/m^2 for (100) Ag/Fe [41]. The sign of interface stress denotes the effect on the thin (or NML) film/substrate system curvature: a negative interface stress makes curvature more convex and produces a tensile force on the constituent layers; a positive one (like in our case) would result in a more concave curvature adding compressive stresses to the layers [38].

4. Discussion

4.1. Variation of Cu and W stress in the as-deposited state

The internal compressive stress state in as-deposited Cu and W (Fig. 9a) is in line with a recent study of Cu/W NMLs consisting of 100

repetitions of 5 nm Cu/5 nm W building layers [14], where W and Cu are also under compression after deposition regardless of the substrate type (Al_2O_3-R and Si(001)+$[Si_3N_5]_{15\ nm}$ substrates).

As it will be discussed in the following, the total internal stress state in as-deposited Cu/W layers includes three different stress contributions: coherency (or lattice mismatch) stress, deposition (or growth) stress and interface stress (presented in Section 3.4).

Coherency stress. All the investigated NMLs, independently of their layer thicknesses, exhibit the same orientation relationship according to Cu{111}<–101>||W{110}<–111> (Fig. 9a). The in-plane interatomic distances along the directions corresponding to the above mentioned relation are: for [–111] W ([–101] Cu) direction (which corresponds to the diagonal of the in-plane hexagon) $d_{Cu} = 2.556$ Å and $d_W = 2.740$ Å [42]. Accordingly, Cu should be under a tensile and W under a compressive stress due to the lattice mismatch (coherency) strain.

Deposition stress. Generally, film deposition by PVD is accompanied by a compressive-tensile-compressive stress transition during consecutive stages of growth (e.g. grains nucleation, coalescence and further coarsening [43]). Magnetron-sputtered W films typically have a compressive deposition stress during the post-coalescence growth stage [44,45]. A tensile to compressive stress evolution for W layers was already observed beyond a thickness of 1 nm [46]. Magnetron-sputtered Cu films with thicknesses in the range of 3–10 nm generally are still in a stage of grain coalescence and the elastic strain energy associated with the minimization of the grain boundary energy then results in a tensile deposition stress [47]. Thus, for the investigated Cu/W layer thicknesses (3, 5, 10 nm), the deposition stress contribution is expected to be tensile for Cu and compressive for W.

According to these two descriptions, coherency and deposition contributions should provide a tensile force in nanoscale Cu layers. However, in all investigated NMLs, Cu is under compression regardless of its layer's thickness, indicating that the interface stress contribution is dominant (note: coherency and deposition stresses for W are both compressive). The impact of the interface contribution should be more pronounced for thinner nano-layers: indeed, the maximal total stress level is found for the thinnest 3Cu/3W NML (–6.7 GPa for W; –2.5 GPa for Cu). In accordance, smaller compressive stresses are observed in the 10Cu/3W and 10Cu/10W NMLs due to the less dominant interface stress contribution for thicker Cu layers. Additionally, an increase of the Cu layer thickness can enhance the misfit dislocation density, thus relaxing stresses in the Cu/W system.

As-deposited 5Cu/5W NMLs with 100 repetitions, as previously investigated in Ref. [14], possess similar W compressive stress level as the 5Cu/5W with 20 repetitions in the present study (~–3.25 GPa). In contrast, the average stress in the Cu layers varies considerably: –1.5 GPa for 100 repetitions against –2.8 GPa for 20 repetitions. This indicates that the number of NML repetitions strongly affects the stress in the Cu layers, whereas the stress in W layers is largely unaffected. This can be related to the higher accumulation of defects during the PVD deposition process for an increasing number of Cu/W bilayer repetitions (from 20 to 100). This results in a stress relaxation, as well due to the formation of misfit dislocations and local thickness variation of the individual Cu and W layers (increase of interface waviness; shown in Fig. 1b). Stress relaxation during the deposition takes place mainly in softer Cu layers, which also can accommodate more defects.

4.2. Stress relaxation by Cu migration prior to NML-to-NC transformation

As described in Section 3, high-temperature annealing triggers the layered structure degradation process and thereby the Cu/W NML-to-NC transformation. It was noted that W compressive stress, in all the NMLs considered in this study, evolves almost monotonically to a zero (or close to zero) stress state with increasing annealing temperature (Fig. 9a). After 800 °C annealing, in all NMLs, with the exception of 10Cu/10W (here the multilayer structure, which is still present, results in a remaining internal stress in Cu and W layers), the W layers are almost stress-free and the original layered structure is completely destroyed. However, Cu preserves a residual final stress state, tensile or compressive (in the NC structure), depending on the NML configuration (Fig. 9a). The more ductile Cu phase should be stress-free at elevated annealing temperatures (700–800 °C). However, a tensile stress resides in the Cu phase of the annealed Cu/W NMLs (700 °C) after cooling down to room temperature (upper panel in Fig. 9a). Considering the relatively small thermal mismatch between W and C-Al_2O_3, any additional stress contribution generated during cooling (due to the thermal mismatch with the Al_2O_3 substrate) will be very small [14]. Hence, the stress in W at the annealing temperature will be very similar to the actual stress measured after cooling down to room temperature. However, the thermal expansion coefficient of Cu is considerably higher than that of W (and of Al_2O_3) [14]. It then follows that, for a stress-free state of W and Cu at elevated annealing temperatures of $T \geq 700$ °C, subsequent cooling can induce a small tensile stress contribution in the confined Cu nano-layers (at room temperature), as observed experimentally (Fig. 9a). The tensile stress level in Cu will be higher for thicker Cu layers, as indeed observed for e.g. 10Cu/10W and 10Cu/3W NMLs (Fig. 9a).

The driving force for the Cu/W NML transformation into a NC structure is provided by the minimization of the total Gibbs energy, as achieved by a reduction of internal interfaces, like high energetic W/W grain boundaries. A similar process of NML structure degradation upon thermal treatment was shown in Ref. [12] for the case of Cu/Co NMLs, in which the diffusion of Cu atoms is aided by the high energy of grain boundaries in Co. The question may be posed why the NML microstructure evolution upon annealing in the present study is not limited only to W self-diffusion and Cu diffusion through the grain boundaries of W, without any Cu surface outflow (protrusions formation). Apparently, higher energy barriers are involved for the compressively strained W layers to transform towards a global system energy minimum, i.e. into a NC structure. Hence, prior to the NML-to-NC transformation, the system tends to release its strain energy stored in the layers after deposition.

Stress relaxation is initiated by the outflow of confined Cu with the formation of protrusions on the NML surface at temperatures as low as 400–500 °C. In Ref. [48], similar Cu outflow was observed in Cu/TiN multilayers under the impact of external compression with concurrent thermal annealing. Moreover, a high density of visible tiny Cu enrichments, concentrated at grain boundaries of coarsened W grains (Fig. 8d) were detected at the NML surface after $T \geq 700$ °C annealing, indicating a thermally activated Cu diffusion process along W grain boundaries at temperatures $T \geq 400$ °C.

Noteworthy, thermally-activated Cu grain-boundary diffusion is accompanied by the simultaneous formation of Cu protrusions at previously formed ruptures of the NML structure (Figs. 5f and 6). Such local ruptures could be induced by creep processes (e.g. dislocation glide, power-law creep, power-law breakdown, diffusional creep). The creep kinetics are influenced by internal stresses, the annealing temperature and the grain size (i.e. the higher internal stresses, smaller grains and higher temperatures promote creep) [49,50]. Enhanced creep due to a combination of higher internal stresses and smaller grains (smaller nano-layer thickness) indeed rationalizes the highest density of surface ruptures and Cu surface particles for the 3Cu/3W NML after annealing at 700 °C (Fig. 7). The lowest density of surface protrusions occurs upon annealing for the 10Cu/10W NMLs due to the higher Cu and W average grain sizes, as well as the lower initial total stress state. The interplay of grain sizes and internal stresses will cause the variation of creep among other NMLs, thus influencing the surface density of Cu protrusions. The STEM analysis (Fig. 6) shows that ruptures are preferentially formed in the top layers of the annealed NML structure, which have a less uniform layer thicknesses and more pronounced interface waviness (Fig. 1b) and thus less required strain for crack formation (shear failure in layers).

Formation of Cu particles in a whisker shape (Fig. 5b,c) at low annealing temperatures (400–500 °C) is due to the presence of an energy barrier for two-dimensional growth of certain facets as mentioned in Ref. [51]. Similar faceting of metallic particles (whisker growth) upon

thermal treatment was observed in Au [52] and Fe [53] systems. At more elevated temperatures (600–700 °C), the activation barrier for nucleation of these high-energy facets is overcome, resulting in a transformation of Cu whiskers into more spherically-shaped Cu particles (Fig. 5d,e).

The observed Cu outflow not only correlates to the stress, but also to the internal disorder. As it is shown in Fig. 9b, for the 3Cu/3W and 10Cu/10W NMLs, internal disorder of the Cu and W layers changes upon thermal treatment. A monotonous decrease of internal disorder with increasing temperature is observed for the Cu layers upon to the onset temperatures for Cu outflow. When Cu surface migration starts, the internal layer disorder is expected to again increase due to the associated atom displacements. No considerable changes of the internal layer disorder are instead observed for W up to the onset temperature of the layer degradation process (700–800 °C). The different responses of the W and Cu layers to the annealing is related to the fact that W is a stiffer material compared with Cu. Indeed their elastic constants, as well as their melting temperatures are in the ratio 3 to 1 [54,55]. Moreover, growth of metallic NMLs by magnetron sputtering is a non-equilibrium deposition process with very high effective temperatures of the adatoms [56]. Using such a non-equilibrium deposition process at low substrate temperatures allows for the kinetic trapping of metastable states (e.g. interface and bulk defects with their associated elastic energy cost) [57]. With increasing annealing temperature, the Cu layers will respond by healing these subatomic displacement defects, while W layers will be less efficient in doing so due to the lower diffusional mobility. Existing domain walls and dislocation edges across as-grown W layers will also remain mostly unchanged.

4.3. Cu particles dissolution at the onset of NML-to-NC transformation

The dissolution of Cu particles formed on the NML surface at $T >$ 700 °C (Fig. 8a) announces the onset of the NML degradation process. As follows from the previous [14] and present studies, W first needs to lower its compressive stress below some critical level (Fig. 9a) to activate thermal grooving of W grain boundaries, inducing pinching-off of the W layers with subsequent spheroidization of residual layer-fragments (Ref. [11] and references within). This thermal grooving is accompanied by the dissolution of previously formed (at 400 °C < T < 700 °C) Cu particles, leading to the NML-to-NC transformation. HR-SEM imaging of 5Cu/5W, 3Cu/3W and 3Cu/10W NMLs annealed at 700 °C reveals that the dissolution process progresses from the Cu particles' edges. Only the 10Cu/3W NML displays extensive Cu particle dissolution without complete NML degradation (at 700 °C). Upon thermal treatment at 800 °C, the Cu protrusions are completely dissolved in all the NMLs. Notably, the layered structure in the annealed 10Cu/10 W NML is still largely preserved after complete Cu particles dissolution (Fig. 3e), also maintaining a high W compressive stress at 800 °C (Fig. 9a), contrarily to the zero W stress state obtained in other NMLs. This is in line with the previous observation that the NML system needs to reach a lower critical stress state in the W layers to advance with the NML-to-NC transformation.

As a rule of thumb, the results of this study show that Cu/W NMLs with higher Cu/W layer thickness ratios (e.g. 10Cu/3W) generally can release their compressive stresses more easily at elevated temperatures. The NC (as formed after complete NML degradation) is stress-free at its transformation temperature. Cooling down to room temperature can induce a slight tensile or compressive stress in the Cu phase, while the W phase remains practically stress-free. Evidently, the Cu/W layer thickness ratio governs the relative volumes and morphologies of Cu and W in the final NC microstructure, as shown in Fig. 3.

5. Summary and conclusion

The impact of the individual Cu and W layer thicknesses on the residual stress and microstructure evolution in Cu/W NMLs upon vacuum annealing (400–800 °C) was investigated.

The individual layer thicknesses were found to determine the magnitude of the initial compressive stress states in Cu and W, thus providing an important tool for stress tailoring in Cu/W NMLs. The high compressive stresses in the as-deposited NMLs can be ascribed to the large interface stress contribution of 11.25 ± 0.56 J/m^2, as pertaining to the Cu(111)/W(110) interfaces.

Thermal treatments allow stress release in the NMLs. The W layers tend to reach a stress-free state after the NML-to-NC transformation, while the stresses in the Cu layers undergo a transformation from compressive to tensile. Four successive stages of the microstructure evolution upon annealing have been identified:

1) Formation of local ruptures of nano-multilayer structure (T < 500 °C).
2) Cu outflow through the ruptures on the nano-multilayer surface, leading to the formation of large Cu particles (400 °C < T < 600 °C).
3) Vanishing (dissolution) of Cu protrusions by means of Cu diffusion back into the volume of Cu/W NML as the onset of the nanocomposite formation (T~700–800 °C).
4) Complete transformation of the NML into a nanocomposite ($T \leq$ 800 °C). The resulting microstructure of the NC largely depends on the initial Cu and W layer thicknesses.

Cu surface outflow provides the main stress relaxation mechanism in the investigated Cu/W NMLs. The kinetics of outflow (onset temperature for the outflow, the size and amount of surface particles) can be tailored by the initial Cu/W stress state and the individual layer thickness ratio. Generally, most intense Cu outflow is observed in NMLs with thin W barrier layers (3 nm) and high internal stresses. Cu whiskers are formed in the range of 400–500 °C, whereas surface protrusions with a more spherical shape develop in the range of 600–700 °C. The onset temperature for NML degradation depends on the individual Cu and W layer thicknesses: a lower thermal stability and faster Cu dissolution occurs for higher Cu/W thickness ratios. NMLs with the higher Cu and W thicknesses (10 nm each) show a preservation of the NML structure up to 800 °C. High stresses in the W layers hinder the onset of the NML degradation process: the stress in W needs to fall below a critical stress level to accelerate W grain coarsening and subsequent nanocomposite formation. The onset temperature for nanocomposite formation also depends on the individual Cu-to-W layer thickness ratio. Overall, the results of this study, provide guidelines for tailoring the onset temperature for nanocomposite formation, as well as the resulting nanocomposite microstructure, in Cu/W NML systems by controlled variation of the individual Cu and W layer thicknesses.

Declaration of interest

The authors declare no conflict of interest.

Acknowledgments

This work was supported by the EU FP7-PEOPLE-2013-IRSES Project EXMONAN – Experimental investigation and modelling of nanoscale solid state reactions with high technological impact (Grant No. 612552); ANII (project FCE-1-2017-1-136126) as well as CSIC and PEDECIBA-Física (Uruguay); COST project IZCNZ0-174856 C16.0075, in the COST Action MP1407 (e-MINDS). The authors are grateful to Dr. Y. Unutulmazsoy, Dr. L. Lin, M. Stiefel, T. Burgdorf, Dr. R. Hauert for technical support and help in the experiments.

Supplementary material

Supplementary material associated with this article can be found, in the online version, at doi:10.1016/j.mtla.2019.100400.

References

[1] J. Janczak-Rusch, G. Kaptay, L.P.H. Jeurgens, Interfacial design for joining technologies: an historical perspective, J. Mater. Eng. Perform. 23 (2014) 1608–1613.
[2] T.W. Barbee, Interfacial effects in multilayers, MRS Proc. 524 (1998) 145–151.
[3] M. Callisti, T. Polcar, Combined size and texture-dependent deformation and strengthening mechanisms in Zr/Nb nano-multilayers, Acta Mater. 124 (2017) 247–260.
[4] P. Kuppusami, G. Balakrishnan, M. Mishra, Microstructure and optical properties of nano multilayers of CeO_2/ZrO_2 and Gd_2O_3/CeO_2 prepared by pulsed laser deposition, J. Nanosci. Nanotechnol. 16 (2016) 10069–10079.
[5] N. Tian, Y. Zheng, Y. He, Z. Dong, H. Jiang, A. Li, S. Yan, H. Wang, Temperature-dependent thermal properties of Ru/C multilayers, J. Synchrotron Radiat. 24 (2017) 975–980.
[6] F.T.N. Vüllers, R. Spolenak, From solid solutions to fully phase separated interpenetrating networks in sputter deposited “immiscible” W-Cu thin films, Acta Mater. 99 (2015) 213–227.
[7] T. Xie, J. Zhu, L. Fu, R. Zhang, N. Li, M. Yang, J. Wang, W. Qin, W. Yang, D. Li, L. Zhou, The evolution of hardness in Cu-W alloy thin films, Mater. Sci. Eng. A 729 (2018) 170–177.
[8] S.J. Lloyd, J.M. Molina-Aldareguia, Multilayered materials: a palette for the materials artist, Philos. Trans. R. Soc. Lond. Ser. A Math. Phys. Eng. Sci. 361 (2003) 2931–2949.
[9] P. Nguyen-Tri, T.A. Nguyen, P. Carriere, C. Ngo Xuan, Nanocomposite coatings: preparation, characterization, properties, and applications, Int. J. Corros. 2018 (2018) 1–19.
[10] Y. Cui, B. Derby, N. Li, A. Misra, Design of bicontinuous metallic nanocomposites for high-strength and plasticity, Mater. Des. 166 (2019) 107602.
[11] F. Moszner, C. Cancellieri, M. Chiodi, S. Yoon, D. Ariosa, J. Janczak-Rusch, L.P.H. Jeurgens, Thermal stability of Cu/W nano-multilayers, Acta Mater. 107 (2016) 345–353.
[12] M. Hecker, J. Thomas, D. Tietjen, S. Baunack, C.M. Schneider, A. Qiu, N. Cramer, R.E. Camley, Z. Celinski, Thermally induced modification of GMR in Co/Cu multilayers: correlation among structural, transport, and magnetic properties, J. Phys. D Appl. Phys. 36 (2003) 564–572.
[13] M. Bobeth, A. Ullrich, W. Pompe, Destratification mechanisms in coherent multilayers, J. Metastable Nanocrystalline Mater. 19 (2004) 153–177.
[14] C. Cancellieri, F. Moszner, M. Chiodi, S. Yoon, J. Janczak-Rusch, L.P.H. Jeurgens, The effect of thermal treatment on the stress state and evolving microstructure of Cu/W nano-multilayers, J. Appl. Phys. 120 (2016) 195107.
[15] W.M. Daoush, J. Yao, M. Shamma, K. Morsi, Ultra-rapid processing of high-hardness tungsten–copper nanocomposites, Scr. Mater. 113 (2016) 246–249.
[16] Z.Y. Zhang, G. Chen, S.L. Zhang, Y.T. Zhao, R. Yang, M.P. Liu, Enhanced strength and ductility in Zrb_2/2024Al nanocomposite with a quasi-network architecture, J. Alloys Compd. 778 (2019) 833–838.
[17] S. Pan, M. Sokoluk, C. Cao, Z. Guan, X. Li, Facile fabrication and enhanced properties of Cu-40 wt% Zn/WC nanocomposite, J. Alloys Compd. 784 (2019) 237–243.
[18] A. Fathy, O. El-Kady, Thermal expansion and thermal conductivity characteristics of Cu–Al_2O_3 nanocomposites, Mater. Des. 46 (2013) 355–359.
[19] S.F. Hassan, M. Gupta, Development of high performance magnesium nanocomposites using solidification processing route, Mater. Sci. Technol. 20 (2004) 1383–1388.
[20] O. Thomas, P. Gergaud, S. Labat, L. Barrallier, A. Charaï, C. Alfonso, B. Gilles, A. Marty, Residual stresses in metallic multilayers, J. Phys. IV 06 (1996) C7–125–C7–134.
[21] F. Moszner, C. Cancellieri, C. Becker, M. Chiodi, J. Janczak-Rusch, L.P.H. Jeurgens, Nano-structured Cu/W brazing fillers for advanced joining applications, J. Mater. Sci. Eng. B 6 (2016) 226–230.
[22] F. Hille, R. Roth, C. Schäffer, H. Schulze, N. Heuck, D. Bolowski, K. Guth, A. Ciliox, K. Rott, F. Umbach, M. Kerber, Reliability aspects of copper metallization and interconnect technology for power devices, Microelectron. Reliab. 64 (2016) 393–402.
[23] J. Baumann, C. Kaufmann, M. Rennau, T. Werner, T. Gessner, Investigation of copper metallization induced failure of diode structures with and without a barrier layer, Microelectron. Eng. 33 (1997) 283–291.
[24] T. Saito, H. Ashihara, K. Ishikawa, M. Miyauchi, Y. Yamada, H. Nakano, A reliability study of barrier-metal-clad copper interconnects with self-aligned metallic caps, IEEE Trans. Electron Devices 51 (2004) 2129–2135.
[25] B. Girault, D. Eyidi, T. Chauveau, D. Babonneau, P.O. Renault, E. Le Bourhis, P. Goudeau, Copper coverage effect on tungsten crystallites texture development in W/Cu nanocomposite thin films, J. Appl. Phys. 109 (2011) 014305.
[26] B. Girault, P. Villain, E. Le Bourhis, P. Goudeau, P.O. Renault, X-ray diffraction analysis of the structure and residual stresses of W/Cu multilayers, Surf. Coat. Technol. 201 (2006) 4372–4376.
[27] M.A. Monclús, M. Karlik, M. Callisti, E. Frutos, J. Llorca, T. Polcar, J.M. Molina-Aldareguía, Microstructure and mechanical properties of physical vapor deposited Cu/W nanoscale multilayers: influence of layer thickness and temperature, Thin Solid Films 571 (2014) 275–282.
[28] U. Welzel, J. Ligot, P. Lamparter, A.C. Vermeulen, E.J. Mittemeijer, Stress analysis of polycrystalline thin films and surface regions by X-ray diffraction, J. Appl. Crystallogr. 38 (2005) 1–29.
[29] P.P. Wang, C. Xu, E.G. Fu, J.L. Du, Y. Gao, X.J. Wang, Y.H. Qiu, The study on the electrical resistivity of Cu/V multilayer films subjected to helium (He) ion irradiation, Appl. Surf. Sci. 440 (2018) 396–402.
[30] T. Wang, Y. Jin, L. Bai, G. Zhang, Structure and properties of NbN/MoN nano-multilayer coatings deposited by magnetron sputtering, J. Alloys Compd. 729 (2017) 942–948.
[31] X. Gao, Y. Fu, D. Jiang, D. Wang, S. Xu, W. Liu, L. Weng, J. Yang, J. Sun, M. Hu, Constructing WS_2/MoS_2 nano-scale multilayer film and understanding its positive response to space environment, Surf. Coat. Technol. 353 (2018) 8–17.
[32] M.J. Pac, Y. Pinot, S. Giljean, C. Rousselot, P. Delobelle, C. Ulhaq-Bouillet, M.H. Tuilier, Investigation of $Ti_{0.54}Al_{0.46}/Ti_{0.54}Al_{0.46}N$ multilayer films deposited by reactive gas pulsing process by nano-indentation and electron energy-loss spectroscopy, Thin Solid Films 634 (2017) 96–106.
[33] A.F. Jankowski, Superhardness effect in Au/Ni multilayers, J. Magn. Magn. Mater. 126 (1993) 185–191.
[34] B.M. Clemens, J.A. Bain, Stress determination in textured thin films using X-ray diffraction, MRS Bull. 17 (1992) 46–51.
[35] M. Jaouen, J. Pacaud, C. Jaouen, Elastic strains and enhanced stress relaxation effects induced by ion irradiation in W(110)/Cu(111) multilayers: comparative EXAFS and x-ray diffraction studies, Phys. Rev. B – Condens. Matter Mater. Phys. 64 (2001) 1–15.
[36] J.A. Bain, L.J. Chyung, S. Brennan, B.M. Clemens, Elastic strains and coherency stresses in Mo/Ni multilayers, Phys. Rev. B 44 (1991) 1184–1192.
[37] R.C. Cammarata, K. Sieradzki, F. Spaepen, Simple model for interface stresses with application to misfit dislocation generation in epitaxial thin films, J. Appl. Phys. 87 (2000) 1227–1234.
[38] J.A. Ruud, A. Witvrouw, F. Spaepen, Bulk and interface stresses in silver-nickel multilayered thin films, J. Appl. Phys. 74 (1993) 2517–2523.
[39] K.O. Schweitz, H. Geisler, J. Chevallier, J. Bøttiger, R. Feidenhans’l, Interface stress and an apparent negative Poisson’s ratio in Ag/Ni multilayers, MRS Proc. 505 (1997) 559–567.
[40] S. Berger, F. Spaepen, The Ag/Cu interface stress, Nanostruct. Mater. 6 (1995) 201–204.
[41] M.R. Scanlon, R.C. Cammarata, D.J. Keavney, J.W. Freeland, J.C. Walker, C. Hayzelden, Elastic and hardness properties of Fe-Ag (001) multilayered thin films, Appl. Phys. Lett. 46 (1995) 46–48.
[42] K. Reshöft, C. Jensen, U. Köhler, Atomistics of the epitaxial growth of Cu on W(110), Surf. Sci. 421 (1999) 320–336.
[43] G. Abadias, E. Chason, J. Keckes, M. Sebastiani, G.B. Thompson, E. Barthel, G.L. Doll, C.E. Murray, C.H. Stoessel, L. Martinu, Review Article: stress in thin films and coatings: current status, challenges, and prospects, J. Vac. Sci. Technol. A Vac. Surf. Film 36 (2018) 020801.
[44] M. Kapp, K.J. Martinschitz, J. Keckes, J.M. Lackner, I. Zizak, G. Dehm, Thermal stresses and microstructure of tungsten films on copper, Berg Hüttenmännische Monatshefte 153 (2008) 273–277.
[45] Y.G. Shen, Y.W. Mai, Q.C. Zhang, D.R. McKenzie, W.D. McFall, W.E. McBride, Residual stress, microstructure, and structure of tungsten thin films deposited by magnetron sputtering, J. Appl. Phys. 87 (2000) 177–187.
[46] L. Wan, X.X. Yu, X. Zhou, G. Thompson, Interrelationship of in situ growth stress evolution and phase transformations in Ti/W multilayered thin films, J. Appl. Phys. 119 (2016) 245302.
[47] T. Kaub, Z. Rao, E. Chason, G.B. Thompson, The influence of deposition parameters on the stress evolution of sputter deposited copper, Surf. Coat. Technol. 357 (2019) 939–946.
[48] R. Raghavan, J.M. Wheeler, D. Esqué-de los Ojos, K. Thomas, E. Almandoz, G.G. Fuentes, J. Michler, Mechanical behavior of Cu/TiN multilayers at ambient and elevated temperatures: stress-assisted diffusion of Cu, Mater. Sci. Eng. A 620 (2014) 375–382.
[49] J.-S. Zhang, High Temperature Deformation and Fracture of Materials, First ed., Woodhead Publishing Limited, Cambridge, 2010.
[50] S. Saha, M. Motalab, Nature of creep deformation in nanocrystalline tungsten, Comput. Mater. Sci. 149 (2018) 360–372.
[51] W.W. Mullins, G.S. Rohrer, Nucleation barrier for volume-conserving shape changes of faceted crystals, J. Am. Ceram. Soc. 83 (2000) 214–216.
[52] A. Kosinova, D. Wang, P. Schaaf, A. Sharma, L. Klinger, E. Rabkin, Whiskers growth in thin passivated Au films, Acta Mater. 149 (2018) 154–163.
[53] D. Amram, O. Kovalenko, L. Klinger, E. Rabkin, Capillary-driven growth of metallic nanowires, Scr. Mater. 109 (2015) 44–47.
[54] H. Huang, F. Spaepen, Tensile testing of free-standing Cu, Ag and Al thin films and Ag/Cu multilayers, Acta Mater. 48 (2000) 3261–3269.
[55] P. Villain, P. Goudeau, P.-O. Renault, K.F. Badawi, Size effect on intragranular elastic constants in thin tungsten films, Appl. Phys. Lett. 81 (2002) 4365–4367.
[56] K. Meyer, I.K. Schuller, C.M. Falco, Thermalization of sputtered atoms, J. Appl. Phys. 52 (1981) 5803–5805.
[57] S. Siol, Accessing metastability in heterostructural semiconductor alloys, Phys. Status Solidi. A (2019) 1–8, 1800858.